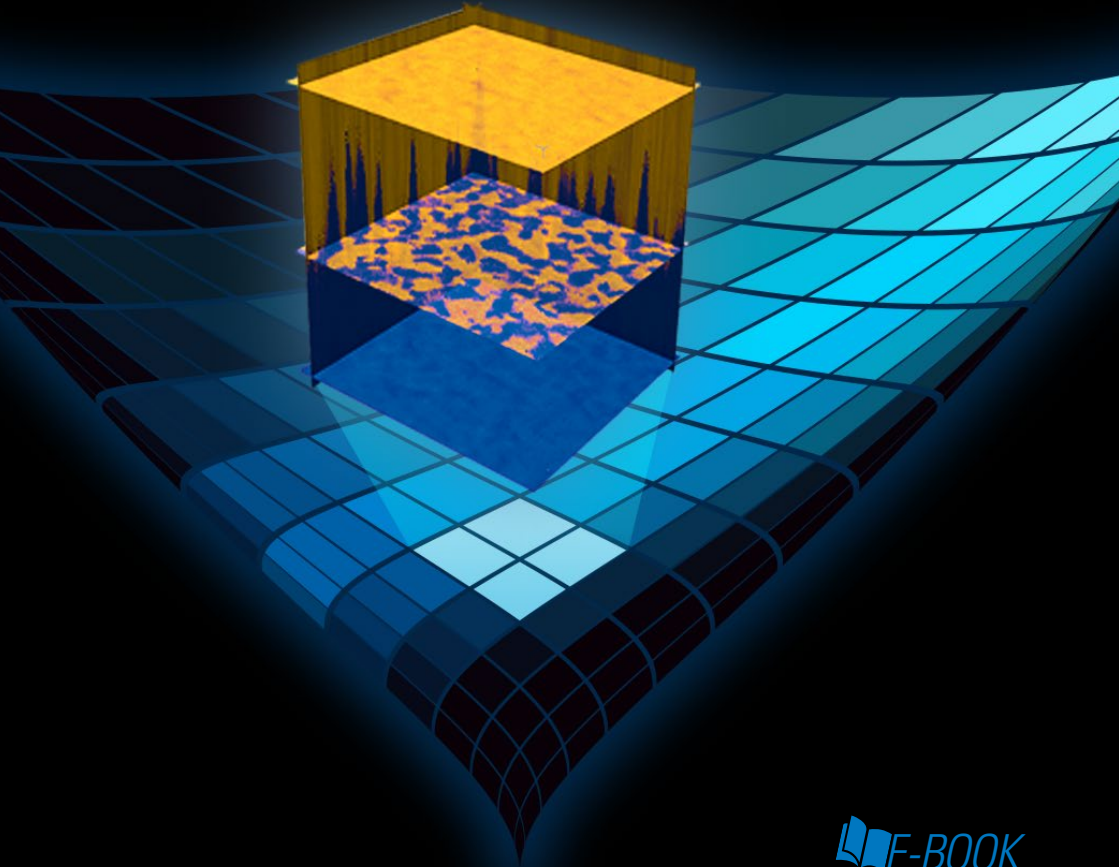


---

The Latest  
**Advances in  
AFM Nanoelectrical  
Modes**

---



## Acknowledgements

Portions of this e-book were sourced with material originally published in:

Li, C., Minne, S. C., Pittenger, B., and Mednick, A., "Simultaneous Electrical and Mechanical Property Mapping at the Nanoscale with PeakForce TUNA," Bruker Application Note 132 (2011).

De Wolf, P., Huang, Z., Pittenger, B., Dujardin, A., Febvre, M., Mariolle, D., and Chevalier, N., "Performing Hyperspectral Mapping with AFM DataCube Nanoelectrical Modes," Bruker Application Note 152 (2019).

# Table of Contents

<b>Acknowledgements</b>	<b>2</b>
<b>Introduction</b>	<b>4</b>
<b>AFM History and Background</b>	<b>6</b>
<b>Extending Property Mapping to Nanoelectrical Analysis</b>	<b>10</b>
<b>Bruker's DataCube Modes</b>	<b>12</b>
<b>DataCube Data Collection</b>	<b>12</b>
<b>DataCube Data Analysis</b>	<b>16</b>
<b>Enabling More Complete Nanoelectrical AFM Research</b>	<b>18</b>
<b>Case Study 1: 22</b>	
DataCube Tunneling AFM on Li-Ion Battery Cathodes	
<b>Case Study 2: 28</b>	
DataCube Scanning Capacitance Microscopy of Semiconductor Devices	
<b>Case Study 3: 30</b>	
DataCube Scanning Microwave Impedance Microscopy on Delicate Samples	
<b>Case Study 4: 34</b>	
DataCube Piezoresponse Microscopy on Piezoelectric Films	
<b>Case Study 5: 40</b>	
DataCube – Contact Resonance PFM on a LiTaO <sub>3</sub> Sample	
<b>Citations</b>	<b>44</b>

## Introduction

Since its initial creation in the early eighties, atomic force microscopy (AFM) has been used in groundbreaking research that in turn has led to a constant stream of new applications. AFM has allowed researchers to map many different sample properties on the micrometer and nanometer levels, which has led to its wide adoption in fields ranging from semiconductors and piezoelectric materials to energy research and biology. As the technology has matured, AFM has given scientists the opportunity to characterize features on ever more complex samples, and not only in topography. Just a few examples include the major and minor groove dimensions of DNA, not just averaged but locally; individual subunits in bacteriorhodopsin, and their stiffness with implications for biological function; molecular scale ordering and properties in polymer interphases; and atomic stiffness in organic and inorganic crystals, and its change at a defect site.

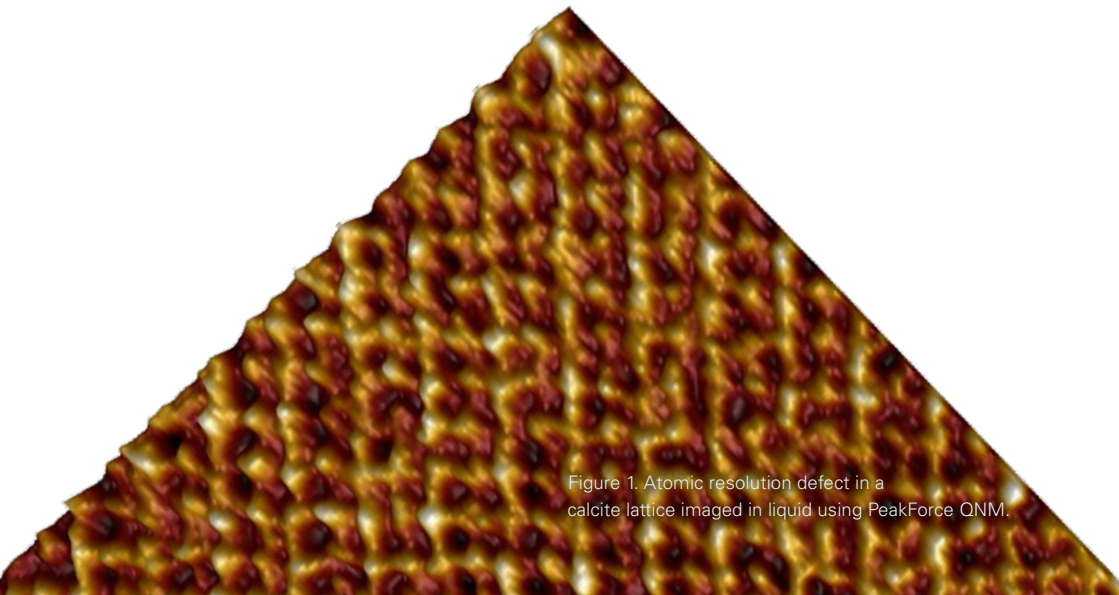


Figure 1. Atomic resolution defect in a calcite lattice imaged in liquid using PeakForce QNM.

The many advances in AFM technology over the past several decades have aimed at extending measurements to applications beyond mere topographic characterization, to soft and fragile samples, and to improving measurement consistency and ease of use. These advancements have not been limited to specific experiments or applications, rather they were general approaches applicable to many applications, including nanoelectrical research, and as such were added to the common analytical toolboxes of researchers.

As an important sub-category, AFM-based nanoelectrical modes have found applications in an ever increasingly wide range of fields and for ever more complex research. Modes are available to characterize the local conductivity, resistivity, charge, carrier concentration, carrier-type, or piezoelectric properties with nanometer-scale spatial resolution, and require a direct contact between the AFM tip and sample.

The data produced have traditionally been in the form of two-dimensional (2D) maps, generated in contact mode, with a single electrical data point per XY location. At a few, carefully selected locations in this map, electrical ramps or spectra are generated to get a deeper insight to the local electrical properties. Bruker has developed a new approach to nanoelectrical imaging that goes beyond a 2D map, creating a correlated electrical and nanomechanical data cube by collecting both electrical and mechanical spectra at each XY location. These new DataCube modes operate at normal imaging speeds and have the added benefit that they avoid contact mode imaging, thus extending electrical measurements to soft and fragile samples and improving measurement consistency through increased tip lifetime. Moreover, taken together, they are a general approach applicable to most nanoelectrical modes and applications. The more complete data sets contain new information and enable functional imaging on complex samples, as shown in examples of barrier height mapping in heterogeneous metal oxides, semiconductor carrier profiling, piezoelectric domain switching dynamics, and Li ion cathode characterization.

After a brief history of AFM, this e-book discusses the technology behind DataCube nanoelectrical modes, how they can be applied to perform hyperspectral mapping, and finally details several case studies to highlight these new capabilities and their wide range of applications.

# AFM History and Background

The scanning tunneling microscope (STM), was developed by Gerd Binnig and Heinrich Rohrer in the early 1980s at IBM Research-Zurich. This precursor work to AFM earned them the 1986 Nobel Prize for Physics. Shortly after, Binnig, Quate and Gerber officially invented the first atomic force microscope and started performing nanoscale research.

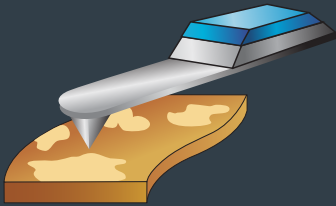
Before AFM, both traditional and specialized optical microscopes were used to investigate surfaces on a small scale. For example, two-photon microscopes were used to map the surfaces of biological samples. Compared to this and other microscopy techniques, AFM uniquely provides surface sensitivity at higher resolution in both the lateral and vertical directions, so that very precise information about the surface topography is obtained.

Early atomic force microscopes used a contact method with a tip mounted to a cantilever to acquire nanoscale sample information. When the tip met the sample's surface, it would bend the cantilever, providing information about the topography of the sample. Commonly referred to as contact mode, this method has certain shortcomings. In particular, contact mode does not control the lateral force between tip and sample, often causing damage to the sample and decreasing tip lifespan.

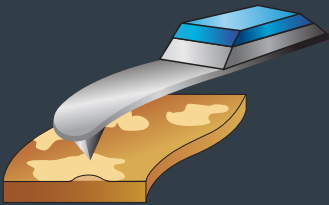
It was quickly realized that there was a need for a less damaging method that could be used with more fragile samples. In 1987, Yves Martin et al. created a non-contact in vacuum method that oscillated the cantilever  $<10$  nm away from the surface of the sample.

AFM has achieved tremendous benefits from a variety of the resulting non-contact oscillating modes of operation, most notably TappingMode, which was introduced in 1993 by Qian Zhong et al for ambient imaging. During TappingMode imaging, the AFM cantilever is oscillated at its fundamental free flexural resonance. This has the advantage of largely eliminating lateral forces that tend to damage the tip and/or sample when imaging in contact mode. The vertical interaction force is also substantially reduced due to the high mechanical  $Q$  of the cantilever, permitting imaging of soft or delicate samples. TappingMode AFM, became immensely popular for a great majority of AFM research, and has remained so even today.

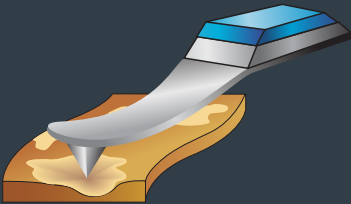
Figure 2. TappingMode operation.



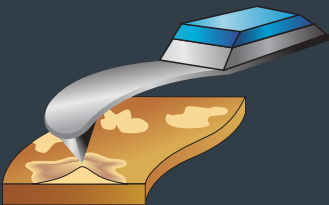
1. Cantilever oscillates in free air. Amplitude is larger than setpoint.



2. Tapping on sample. Cantilever oscillates at setpoint amplitudes.



3. Tip encounter a particle. Cantilever oscillation amplitude drops.



4. Feedback lifts the Z piezo. Amplitude returns to setpoint.

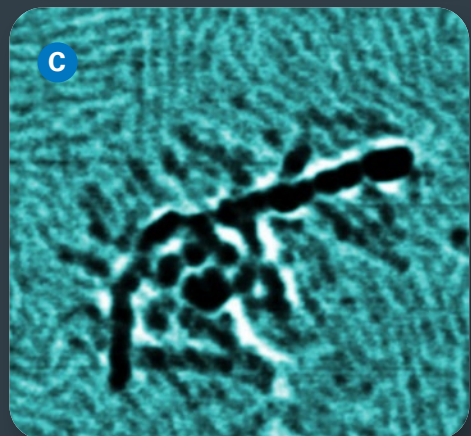
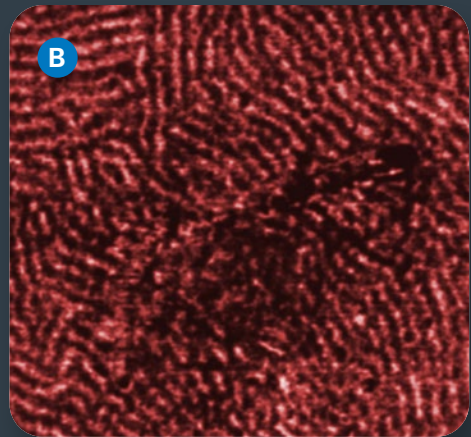
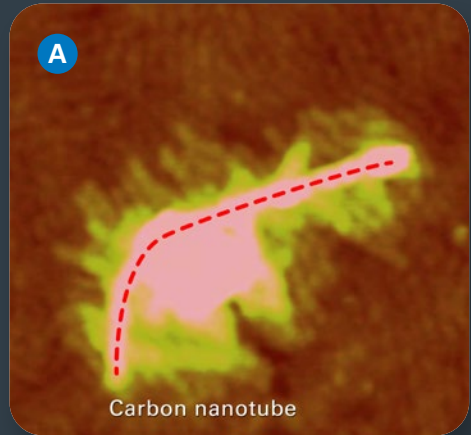
Over the next 15 years, various contact and tapping modes using a conductive tip extended AFM applications from topographic images to electrical surface characterization, resulting in many new avenues of research. For example, conductive AFM (C-AFM) is a secondary imaging mode derived from contact mode that characterizes conductivity variations across medium- to low-conducting and semiconducting materials. It is used to measure and map current in the 2pA to 1 $\mu$ A range while simultaneously collecting topographic information. Tunneling AFM (TUNA) works similarly to C-AFM but characterizes the ultra-low currents down to hundreds of fA that pass through the thickness of thin films, and is of particular importance when electrical characterization of low-conductivity samples is needed at high lateral resolution. Scanning capacitance microscopy (SCM) provides a method for direct measurement of activated carrier concentration with nanometer scale accuracy in two dimensions.

Over this time period, there were many other incremental innovations in both AFM hardware and mode capabilities and usage that contributed to an ever growing body of AFM research. The development of PeakForce Tapping® in 2009 was a culmination of many of these advances, and has in turn led to thousands of publications and a large family of new derivative modes. As with TappingMode, the probe and sample are intermittently brought into contact while the tip is scanned across the sample to eliminate lateral forces during imaging. Unlike TappingMode, where the feedback loop keeps the average cantilever vibration amplitude constant, in PeakForce Tapping the feedback loop controls the maximum force on the tip (peak force). Because the force measurement bandwidth of a cantilever is approximately equal to its fundamental resonant frequency, by choosing a modulation frequency significantly lower than the cantilever's resonant frequency, the PeakForce Tapping control algorithm is able to directly respond to the tip-sample force interaction. This direct force control protects the tip and the sample from damage, but more importantly, allows every tip-sample contact to be recorded for additional mechanical property analysis. PeakForce Tapping has led to a host of nanomechanical research advances and new characterization modes over the last 10 years.



Figure 3. PeakForce TUNA (A) topography, (B) current, and (C) adhesion maps of a semiconducting polymer composite, poly(3-hexylthiophene) (P3HT) with embedded carbon nanotubes. The current map shows conductivity at the level of individual lamellae. In contrast, contact mode based approaches fail to achieve this resolution due to sample damage from lateral forces.

Image courtesy of Philippe Leclère et al, University of Mons (UMONS) Belgium.



## Extending Property Mapping to Nanoelectrical Analysis

The ability to simultaneously capture and extract mechanical properties from the tip-sample interactions with PeakForce Quantitative Nanomechanics (PeakForce QNM®)<sup>1-4</sup> and FASTForce Volume™ (FFV)<sup>5</sup> modes provide an entire force curve for every pixel of the image, and the contact resonance mode<sup>5</sup> provides a resonance spectrum for every pixel of the image. From these spectra, mechanical properties such as adhesion, stiffness, modulus, deformation, tan-delta, and loss and storage modulus can be extracted and visualized in two-dimensional (2D) maps.

For electrical characterization, a range of application modules have been developed,<sup>6-9</sup> and even electrical measurements in liquid are possible with the recent introduction of insulated AFM nanoelectrode probes for scanning electrochemical microscopy (SECM) and nanoelectrical characterization.<sup>10-14</sup> Combining all of these capabilities within single AFM platforms has provided researchers greater efficiency and experimental reach in both routine industrial applications and for highly multidisciplinary research in piezoelectricity, semiconductor devices, polymeric systems, energy research, and materials characterization.

Conventional AFM nanoelectrical modes are generally operated with a fixed set of operating conditions (DC bias, AC bias, frequency, etc.) and a single electrical measurement is performed for every XY location, yielding a 2D electrical map. This is also true in PeakForce Tunneling AFM (PeakForce TUNA™) and related PeakForce Tapping-based electrical modes, which overcome the limitations of contact mode. Aside from 2D maps, AFM-based electrical characterization has long included point spectroscopy, whereby one of the operating conditions is swept as the tip is kept stationary, for example in the acquisition of current-voltage (I-V) curves at a single or a few selected individual positions. Point spectra can also be performed in arrays, but until now, this has remained rather time-consuming and has only allowed limited spatial sampling. Published application examples include capacitance-voltage (C-V) spectra applied for studying pn-junction delineation in Si devices,<sup>15</sup> and I-V spectra for investigating humidity effects on nanoscale electrochemistry in solid silver ion conductors.<sup>16</sup>

Figure 4. Height (A) and current (B) maps of a carpet of vertical carbon nanotubes, obtained with PeakForce TUNA. Because the sample is very fragile, it is impossible to image with contact mode. Image size 1  $\mu\text{m}$ .

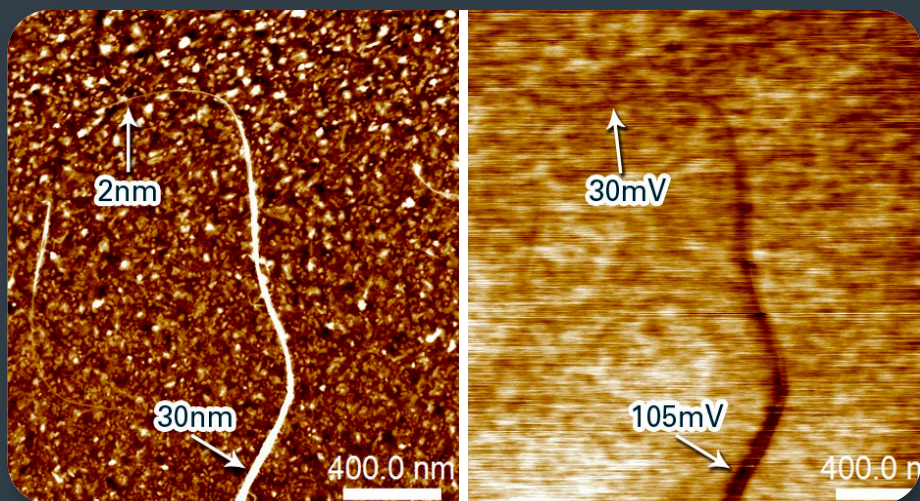
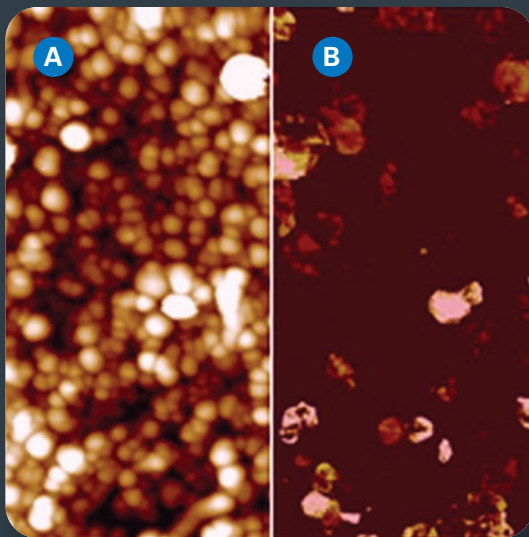


Figure 5. Height (left) and PeakForce KPFM potential (right) map of single-walled carbon nanotubes (SWCNTs) laid on a Si substrate. A single strand CNT (pointed to by the upper arrow) sticks out of a CNT bundle (pointed to by the lower arrow), which can be resolved in potential map, but no longer with accuracy as the dimension is too small to give dominant contribution in frequency modulation KPFM.

## Bruker's DataCube Modes

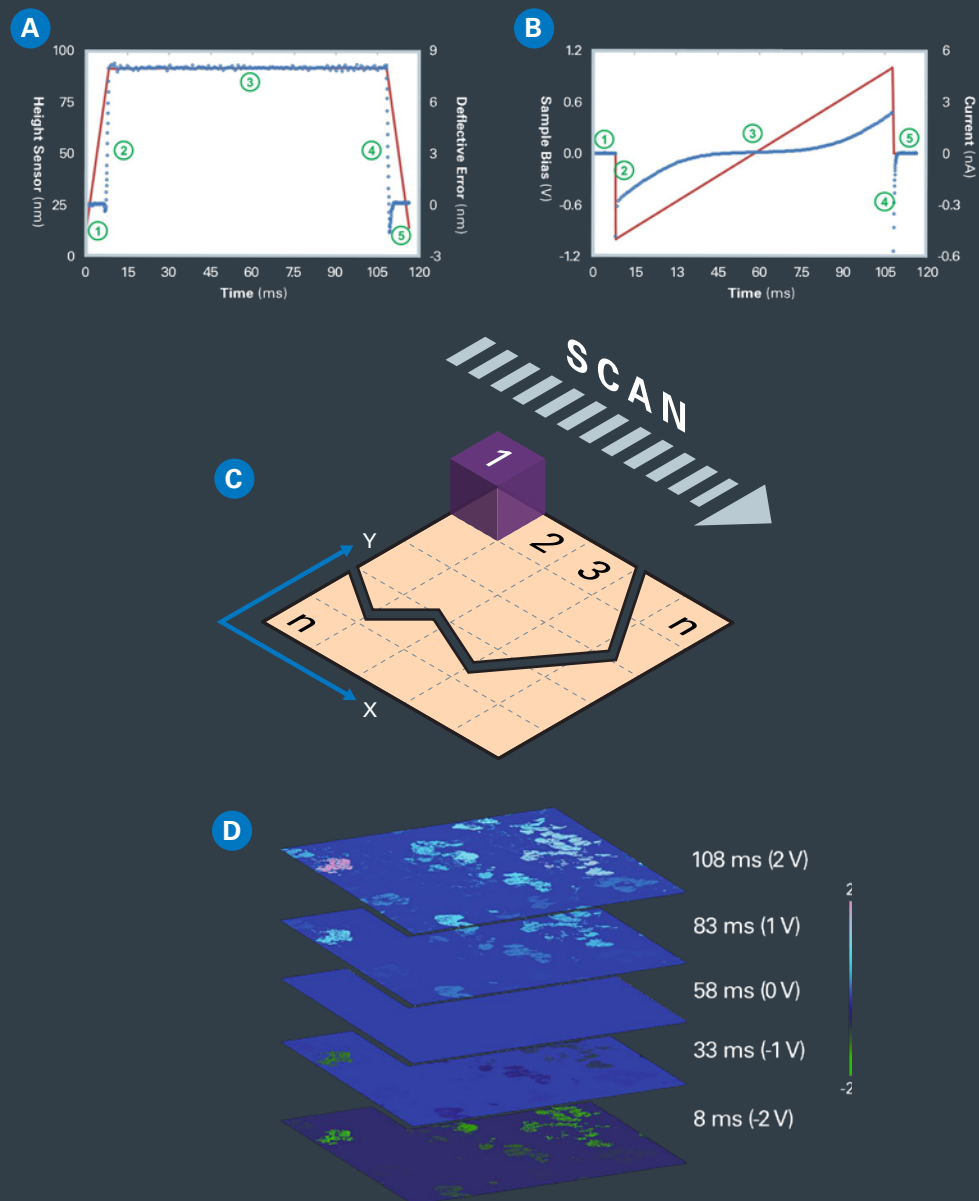
Bruker has taken nanoelectrical analysis considerably further with its development of data cube technology, which combines the benefits of both the traditional AFM imaging modes and point spectroscopy to create 3D results quickly from nanoelectrical data. These multidimensional data cubes measure the dependence of a specific electrical parameter in each XY position as a function of one of the (electrical) operating conditions.<sup>17</sup> The common subjective approach of guessing locations of interest (for single-point spectroscopy) is replaced by a big data approach, resulting in higher dimensional data that can be sliced along any axis or plane.

The high dimensional electrical data sets allow one to extract high-resolution maps of electrical properties previously not acquired using AFM. Examples include images of Schottky barrier height, flat-band voltages, and piezoelectric switching voltages. Rather than employing contact mode, the tip is moved from pixel to pixel in a FFV method. An electrical spectrum is acquired during a hold segment inserted into each force curve in each pixel. The force curve at every pixel embedded in the FFV map constitutes a set of nanomechanical data cubes, which are spatially correlated with the electrical data cubes. Since the FFV map avoids lateral forces, tip lifetime is drastically improved and the electrical measurements are extended to polymers, nanoparticles, and other fragile samples that are impossible to study in contact mode.

## DataCube Data Collection

Bruker's DataCube (DCUBE) modes are the result of seamless integration of existing high-performance nanoelectrical modes with the FFV technique. In the FFV mode, the tip is held in a fixed XY position, while a force distance cycle with *dwell* segment is executed in the Z direction. This is illustrated by the height sensor plot and corresponding force curve shown in Figure 6. Force ramp rates up to 300 Hz are possible using Bruker's proprietary low-force trigger capability. Combined with sub-100 ms dwell times for the hold segment, good throughput is obtained, and one can maintain regular imaging speeds also when acquiring dense arrays. In Figure 6, the ramp rate for the *extend* and *retract* segments is 60 Hz at a normal force (or deflection) trigger level of 15 nN and with a Z movement of 80 nm. This results in a ramp speed of 9.6  $\mu\text{m/s}$ .

Figure 6. DataCube modes operating on FASTForce Volume approach: (a) height sensor (red) and deflection error (blue open circle) plots with segments showing extend (1–2), dwell (3), and retract (4–5) cycles; (b) pattern of sample bias (red) and corresponding TUNA current (blue); (c) illustration of scan pattern during acquisition of DCUBE-mode data; and (d) five TUNA current slices from the DCUBE-TUNA results.



During the dwell segment (here 100 ms), the sample bias is swept from -2 V to +2 V, corresponding to a ramp rate of 40 V/s. The number of data points for the non-dwell and dwell segments can be set independently, allowing for high spectral resolution. In this example, 256 and 190 data points result in resolutions of 0.625 nm in Z and 21 mV in sample voltage, respectively. Higher density can be obtained by further increasing the amount of data points. The four spectra (height, deflection error, sample bias, and TUNA current) are captured simultaneously. After acquisition of the spectra in one pixel, the tip is retracted from the surface before moving to the next pixel using the FFV raster scanning method (Figure 6c). This avoids the shear force mentioned earlier that is common in contact mode-based scanning. Figure 6d shows five typical current slices extracted from a data cube acquired using this principle on a  $\gamma$ -Fe<sub>2</sub>O<sub>3</sub> sample. Each current slice image consists of 256x256 pixels for a sample area of 3x3  $\mu\text{m}^2$ . The 190 spectral data points from the dwell segment provide 190 of these current slice images. At the same time, the extend/retract segments of the deflection plot construct a complete force-distance curve and allow one to extract quantitative nanomechanical images for modulus, adhesion, deformation, and stiffness.

In DataCube modes, the conditions for force curve cycle and the electrical dwell period are controlled separately. This allows users to independently fine tune the measurement of force-distance spectra and electrical spectra. The duration of the hold segment for good quality signals depends on the nanoelectrical mode in use. More specifically, it depends on the applied AC frequency and/or the bandwidth of the sensor. As sensors normally have a bandwidth in the kilohertz range (for example; the PeakForce TUNA application module has a typical bandwidth of 15 kHz), acquisition times for capturing the whole electrical spectrum down to millisecond level are possible. For example, a dwell time of 50 ms or a ramp rate of 80 V/s is sufficient to capture all the spectral features of the sample in Figure 7. Considering both force and electrical spectra, the time per pixel is typically in the range of 20 to 200 ms. For a 256x256-pixel map, this corresponds to an acquisition time of 22 to 220 minutes. Albeit, with this relatively long spectroscopic mapping duration, one can capture more than 1000 data points for each electrical spectrum, resulting in more than 1000 dynamic sequence or slice images at a capture rate of 1.3 to 13 seconds per image.

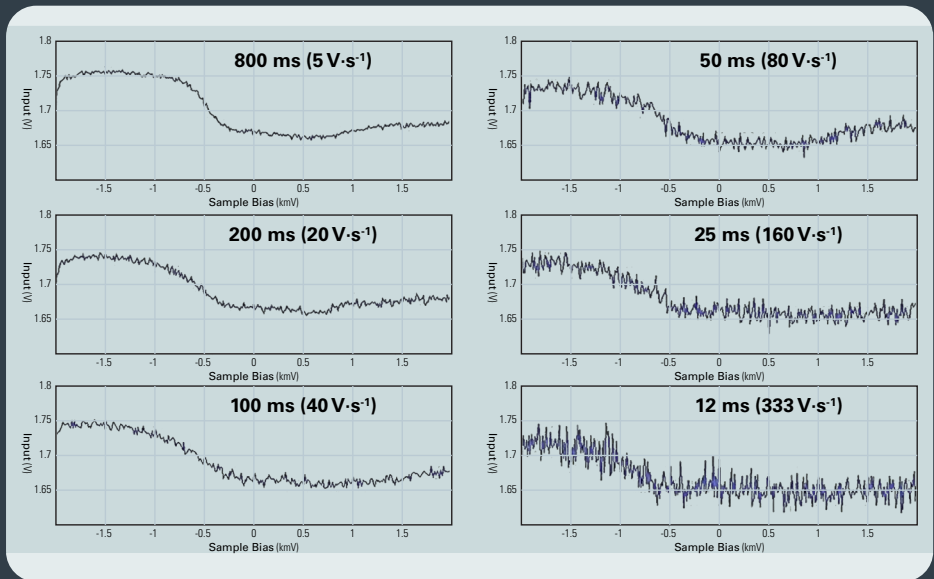


Figure 7. A series of C-V spectra of a p-type semiconductor captured by DCUBE-sMIM. These are raw data without averaging. The dwell time and the sample bias ramp rate for each spectrum are indicated.

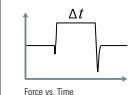
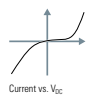
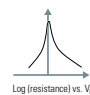
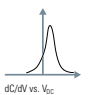
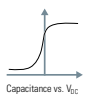

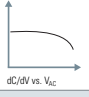
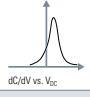
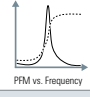
Mechanical		Electrical				
	Force Volume	DCUBE-TUNA	DCUBE-SSRM	DCUBE-SCM	DCUBE-sMIM	DCUBE-PFM
Ramp Parameter	Distance	$V_{DC}$	$V_{DC}$	$V_{DC}$ $V_{AC}$ $f_{AC}$ Phase	$V_{DC}$ $V_{AC}$ $f_{AC}$ Phase	$V_{DC}$ $V_{AC}$ $f_{AC}$ Phase
Output Channel	Force Stiffness Adhesion Modulus	Current	log(Resistance)	dC/dV Amplitude dC/dV Phase	dC/dV Amplitude dC/dV Phase sMIM-C sMIM-R	PFM Amplitude PFM Phase
Example Spectra						
						

Figure 8. Summary of DCUBE modes and electrical characterizations with FFV.

As an alternative to ramping the DC sample bias during the dwell period, the user can also select to ramp any other parameter relevant to the electrical mode selected (e.g., the AC voltage, amplitude or frequency). In this way, one can collect a wide variety of electrical spectra, including I-V, C-V, dC/dV-V, R-V, dR/dV-V, PFM-amplitude-V, and PFM-amplitude-frequency spectra. Figure 8 summarizes the available electrical DCUBE modes.

The electrical conditions can also be held constant during the dwell period, which can be short (milliseconds) or long (tens of seconds), and varies in a similar way to the shutter speed on a camera. In this way, the electrical signal can be averaged over a user-defined period, resulting in improved signal/noise ratios as compared to the equivalent contact or PeakForce electrical mode. During the dwell period, the electrical parameter is measured as a function of time, opening up the possibility to study time-dependent phenomena. Examples include mapping of time-dependent conductivity or photoconductivity after an external stimulus, such as a light pulse or electrical pulse; observing time-dependent dielectric breakdown in dielectrics; and investigating charging or discharging effects after applying a voltage pulse.

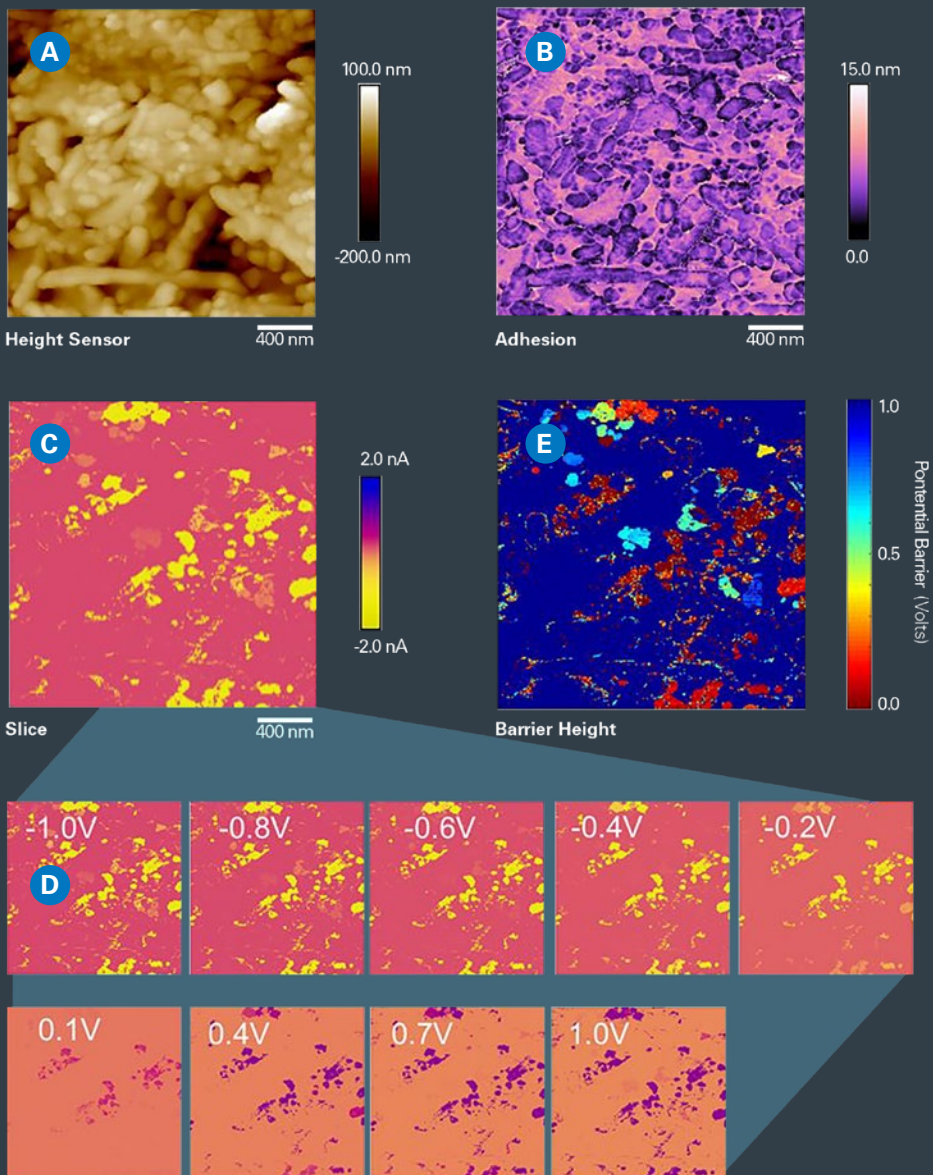
## DataCube Data Analysis

After acquiring the data, it needs to be analyzed. This is where the different DataCube modes truly excel, as they provide simultaneous capture of nanometer-scale electrical and mechanical characteristics in high-density data cubes. For materials scientists and engineers, this breaks long-standing efficiency and characterization barriers. Processing such information-rich, big data results stimulates and encourages creative data mining. Bruker's standard NanoScope® analysis offline software provides a suite of data tools for basic processing and visualization, such as the extraction of individual slices and spectra. Figures 9 and 10 illustrate some of the core functions for handling DataCube data (here, applied to DCUBE-TUNA data acquired on a  $\gamma$ -Fe<sub>2</sub>O<sub>3</sub> sample).

First, slices of the spectroscopic maps can be extracted for further processing, as one would do with regular AFM images. This allows surface topography and quantitative nanomechanical maps to be extracted, as shown in Figures 9a and 9b. Figure 9c shows a current slice at a fixed sample bias of -1 V, while Figure 9d shows more current slices at nine selected



Figure 9. Processing, analysis, and visualization of DCUBE data. Slices of the spectroscopic maps can be extracted for regular processing of AFM images in NanoScope Analysis software: (a) surface topography; (b) quantitative nanomechanical properties—adhesion map; (c) a slice map from TUNA current—sample bias (I-V) spectra at -1 V (cover image of a movie created from 130 slices available on the Bruker website); (d) slices of TUNA current maps at selected voltages; and (e) scanning barrier height images created by analyzing all I-V spectra. The color bar displays from ohmic (zero) to insulating (one).



voltages. Figure 10a shows a current slice at +2 V collected in a different area on the  $\gamma$ -Fe<sub>2</sub>O<sub>3</sub> sample.

Second, one can select, display and export any of the spectra through single or multiple point selection in the surface topography, nanomechanical, or nanoelectrical images. One can also display and overlay all spectra from a selected region. Such a dense collection of spectra can also be visualized through statistical methods with the built-in density plots. An example is shown in Figure 10c created from 1890 spectra in the dashed-yellow-square region in Figure 10a. The darkness in this plot corresponds to the population density of the spectrum in this region of interest. In this particular example, the three visible curves in Figure 10c indicate three distinct electrical domain behaviors: insulating, low barrier, and high barrier.

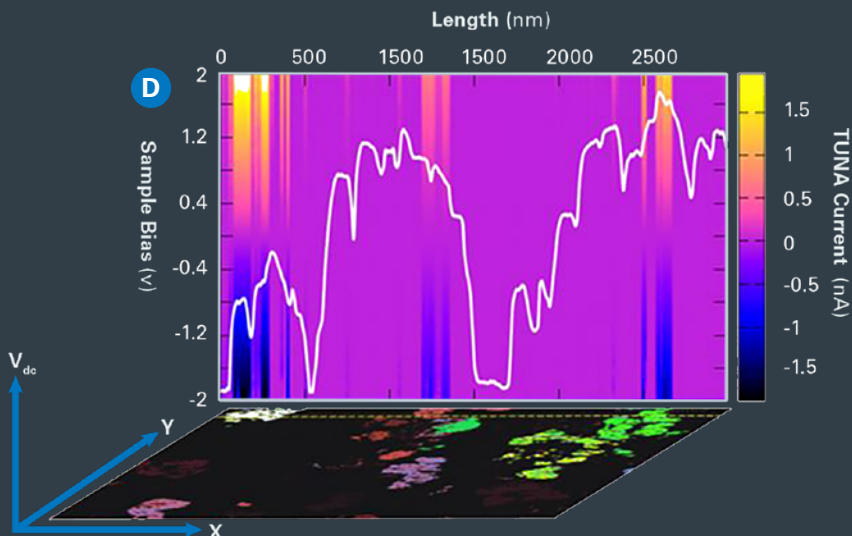
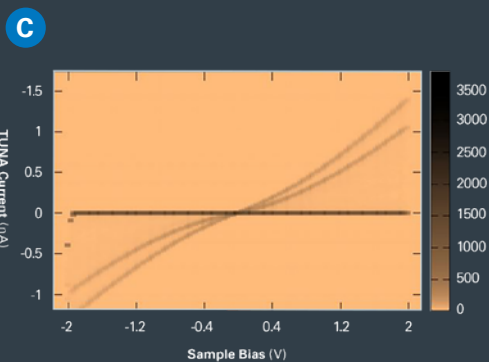
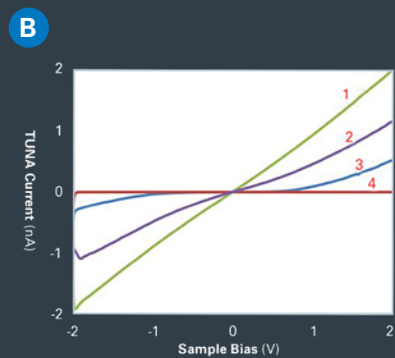
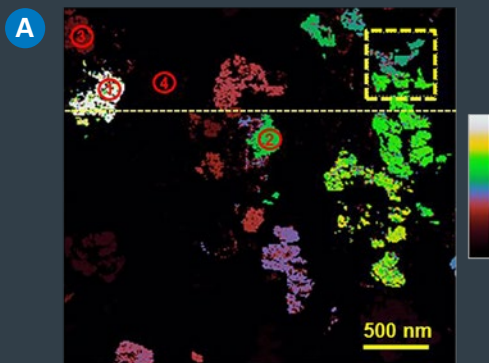
Third, the analysis software can also provide electrical contour plots along a user-defined line. Figure 10d shows the TUNA current changes over sample bias across the dashed-yellow line in Figure 10a. This is a 2D slice of the data cube at a fixed Y position, as indicated by the coordinates on the image. Each vertical line contains spectral information rendered by the false color of TUNA current. The (dark) blue-to-yellow stripes indicate the location along the line in Figure 10a where TUNA current changes with sample bias. The white plot on Figure 10d is the corresponding surface profile along the dashed-yellow line in Figure 10a, with a range of 150 nm in height. This shows that the nanoelectrical properties have no clear correlation with the surface topography and are only randomly varied among different particles.

## Enabling More Complete Nanoelectrical AFM Research

This e-book has given both an overview of nanoelectrical AFM technology and an in-depth explanation of the new DataCube modes. From the general history of AFM to the more specific data collection and analysis, one can see the tremendous advantage that current state-of-the-art nanoelectrical AFM research can provide.

DataCube-based nanoelectrical modes represent a big data approach with the potential to provide new information in a wide range of applications,

Figure 10. Processing, analysis, and visualization of nanoelectrical data from DCUBE-TUNA mode with NanoScope Analysis software: (a) current slice at +1 V; (b) point-selected I-V spectra as numbered in (a); (c) density plots based on 1890 I-V spectra from the dashed-yellow-square region in (a); and (d) TUNA current changes over sample bias across the dashed-yellow line in (a) where the white plot on the image is the corresponding surface profile with a range of 150 nm in height. This is a two-dimensional slice of the data cube at a fixed Y position as indicated by the coordinates on the image.



especially on samples with high complexity. Extracting image slices, spatio-spectral slices, or spectra at every pixel opens the door to reveal sample properties that are either not accessible or are easily missed by conventional electrical characterization techniques.

Advantages include large data content with full spectral information and images at a range of operating conditions, correlation between electrical and mechanical properties, longer tip lifetime, the capability to measure soft and fragile samples, and mapping of new nanoelectrical properties. The following case studies highlight a few specific nanoelectrical research examples that showcase the data cube approach.



# Case Study 1:

## DataCube Tunneling AFM on Li-Ion Battery Cathodes

One problem that can be approached with DataCube technology is the failure of Li-ion battery cathodes. Li-ion battery cathodes have multiple components of different properties, some more easily damaged than others. PeakForce Tapping with DataCube analysis allows us to avoid incurring typical damage from contact mode, while DataCube analysis allows us to look at the conductivity of single grains in the sample.

The failure of Li-ion battery cathodes results from complex interrelated phenomena. It depends on battery chemistry, design, environment, and actual operation conditions.<sup>18</sup> Therefore, understanding, improving, and controlling the lifetime and performance of a battery requires studies at the component level. AFM has proven to be a powerful instrument for battery component studies.<sup>19</sup> However, the presence of materials with distinct mechanical properties, from soft (polymer additive), loose (conductive additive), to hard (Li metal oxide), porous (separator) surfaces, and high variation in surface topography, can pose challenges for contact-based scanning modes due to the nature of high normal imaging force and shear force.

TappingMode is superior to contact mode surface mapping in regard to high variation in mechanical properties. However, a majority of nanoelectrical characterization is based on solid tip-sample contact. Recently, PeakForce Tapping modes have proven useful for imaging challenging samples like battery materials,<sup>20-24</sup> in particular for in situ studies of the fragile solid electrolyte interphase layer on both anodes<sup>25-27</sup> and cathodes.<sup>28, 29</sup> DataCube modes further expand the capabilities of PeakForce Tapping modes by enabling the acquisition of multidimensional data cubes through simultaneous capture of nanometer-scale electrical and mechanical characteristics in high-density data cubes.

The cathode investigated in this example consists of Li metal oxide, polymer binder, and conductive carbon nanoparticles. First, a large area of  $45 \times 45 \mu\text{m}^2$  was scanned, which can be challenging for other AFM nanoelectrical methods on this type of composite sample. Figure 11a shows a high-quality image of surface topography. The variation in height is over  $1 \mu\text{m}$ , which is

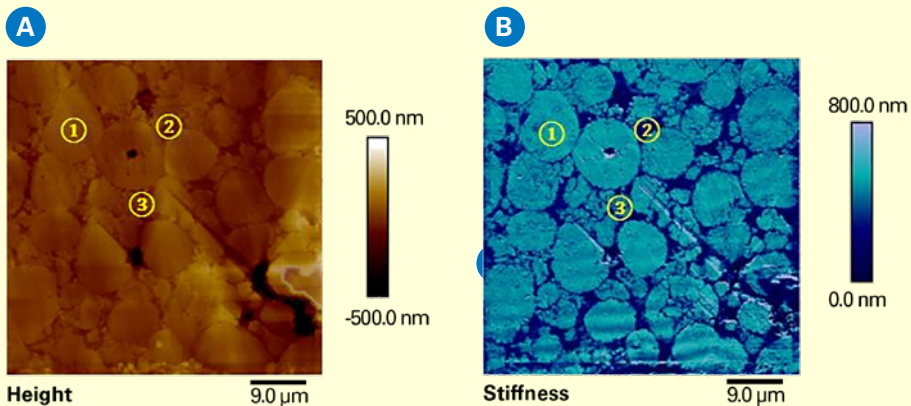
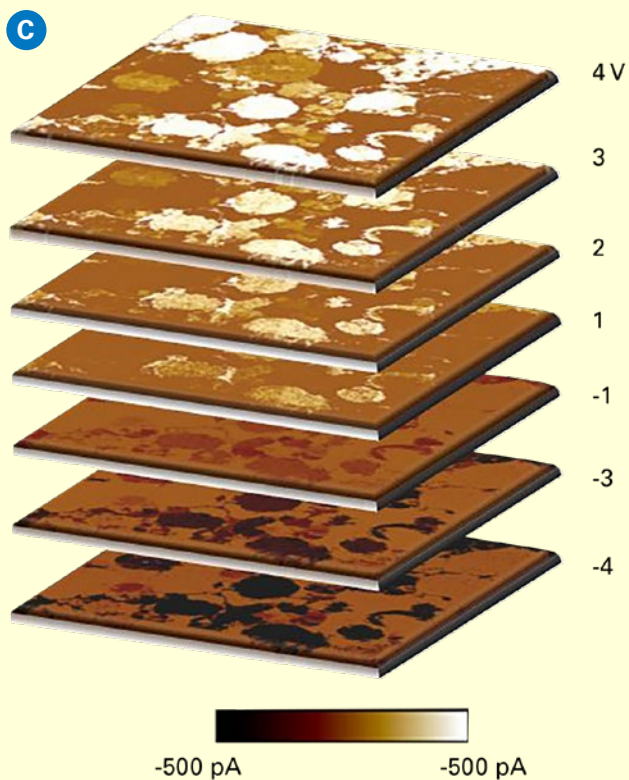


Figure 11. DCUBE-TUNA study of a battery cathode consisting of Li metal oxide (1), polymer binder (2), and conductive carbon nanoparticles (3): (a) surface topography; (b) quantitative surface stiffness differentiating different domains; and (c) a collection of TUNA current slices from the spectroscopic mapping at selected sample voltages. The scanning area is  $45 \times 45 \mu\text{m}^2$ .



typical for a Li-ion battery cathode. Representative domains of Li metal oxide, polymer binder, and carbon black are indicated on the images.

The different domains are better identified by Figure 11b, a quantitative map of surface stiffness, as Li metal oxide is one of the hardest materials, and it shows the highest stiffness, whereas the polymer binder is the softest with the lowest stiffness. Figure 11c is a collection of slices from the spectroscopic mapping, showing the TUNA current image at selected sample bias, as indicated to the right. These TUNA current maps clearly show distinct conductivities over different material domains, as well as conductivity heterogeneity over different Li metal oxide grains.

Figure 12 shows more details about this sample with a scan size of  $15 \times 15 \mu\text{m}^2$ , where the different material domains and the heterogeneity over different Li metal oxide grains are further presented. Figure 12a is the surface topography showing a few large Li metal oxide grains, e.g., regions #1–3. The inter-grain filling materials are difficult to identify on this morphology map. This is partially addressed by the stiffness and modulus maps in Figures 12b and 12c, where Li metal oxide shows high stiffness and modulus, respectively. This differentiation is confirmed by the TUNA current map in Figure 12d, a slice of spectroscopic mapping at a sample bias of +4 V.

Carbon black rich regions (region #5) show high conductivity, while polymer binder regions are insulating (region #4). For the Li metal oxide domains, it is interesting that grain #2 only shows background current, which is totally different from other grains. This could be due to the lack of conduction channel connected by carbon black additives or by the intrinsic nature of the grain itself. Such a region needs to be avoided in practical design as it only serves as a redundant weight and volume burden to the battery, lowering the specific energy or volumetric energy density. In addition, the Li metal oxide also shows inner-grain heterogeneity, as indicated by grain #3 on Figure 12d. Figure 12e is a collection of slices from the spectroscopic mapping showing TUNA current images at selected sample biases as indicated. This series of images further confirms the electrical properties. More importantly, it shows the dynamic changes with applied sample biases from -4 V to +4 V. The current-voltage behaviors of the Li metal oxide grains deviate from linear Ohmic response. For example, the cathode is relatively silent to sample bias from -0.5 V to +0.25 V.



Figure 12. DCUBE-TUNA study of a battery cathode consisting of Li metal oxide (1)-(3), polymer binder (4), and conductive carbon nanoparticles (5): (a) surface topography; (b) quantitative surface stiffness differentiating different domains; (c) quantitative modulus map; and (d-e) TUNA current slices from the spectroscopic mapping at selected sample voltages. The scanning area is 15x15  $\mu\text{m}^2$ .

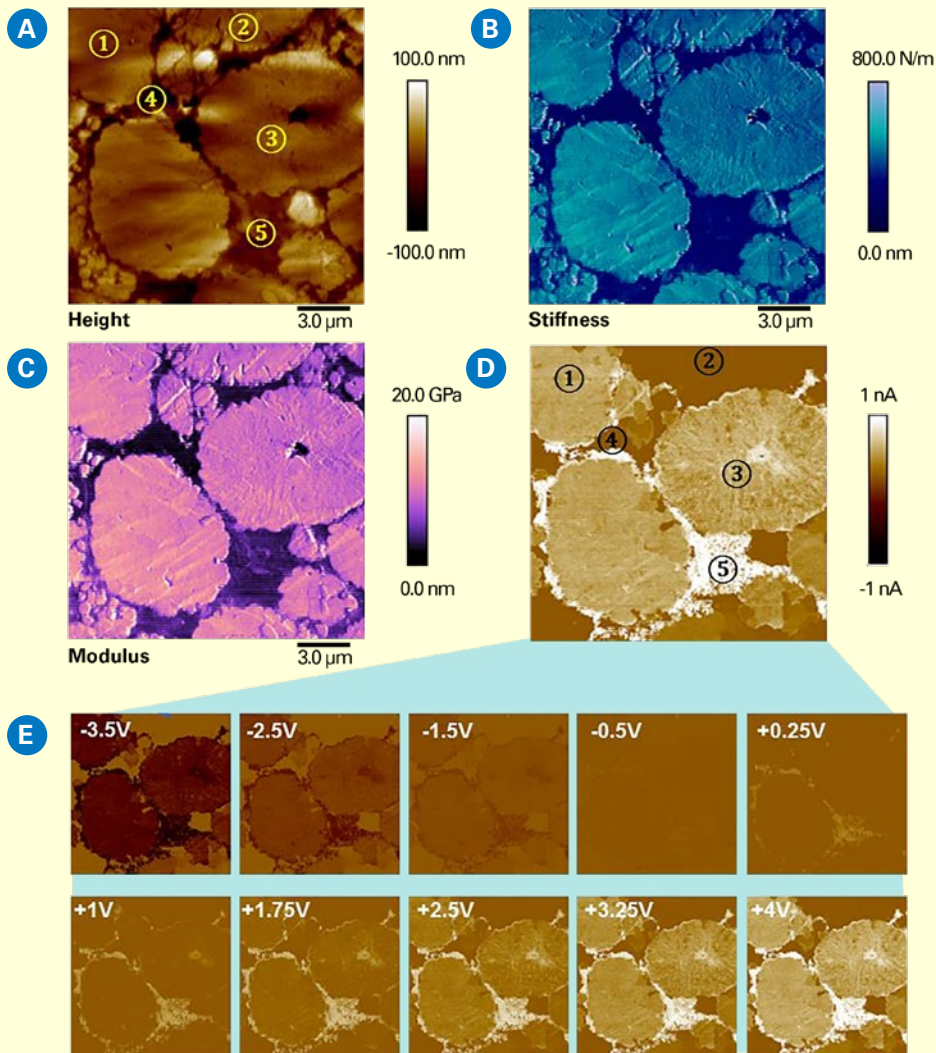


Figure 13 shows the DCUBE-TUNA results of a single Li metal oxide grain on this cathode. Surface topography in Figure 13a shows that this grain is an aggregate of sub-micron nanoparticles that have similar mechanical properties, as shown in the stiffness (Figure 13b) and modulus (Figure 13c). The TUNA current slices in Figures 14d and 14e extracted from the DCUBE-TUNA spectra at sample biases of +4 V and -4 V show conductivity variations amongst these particles. This confirms the inner-grain electrical heterogeneity shown in Figure 12d.

Figure 13f plots all current-time spectra from the area indicated by the white square in Figure 13e. During this 125 ms dwell period, the sample bias sweeps linearly from -4 V to +4 V, or at a rate of 64 V/s. The square area is across two nanoparticles with different conductivities, as shown in Figure 13e. Within each particle, the conductivity is relatively homogeneous. This results in two distinct groups of spectra, as shown in Figure 13e.

This example illustrates that DataCube imaging provides dynamic, multidimensional information for clearly differentiating and analyzing the performance of a complex system constructed from functional materials with distinct physical properties.

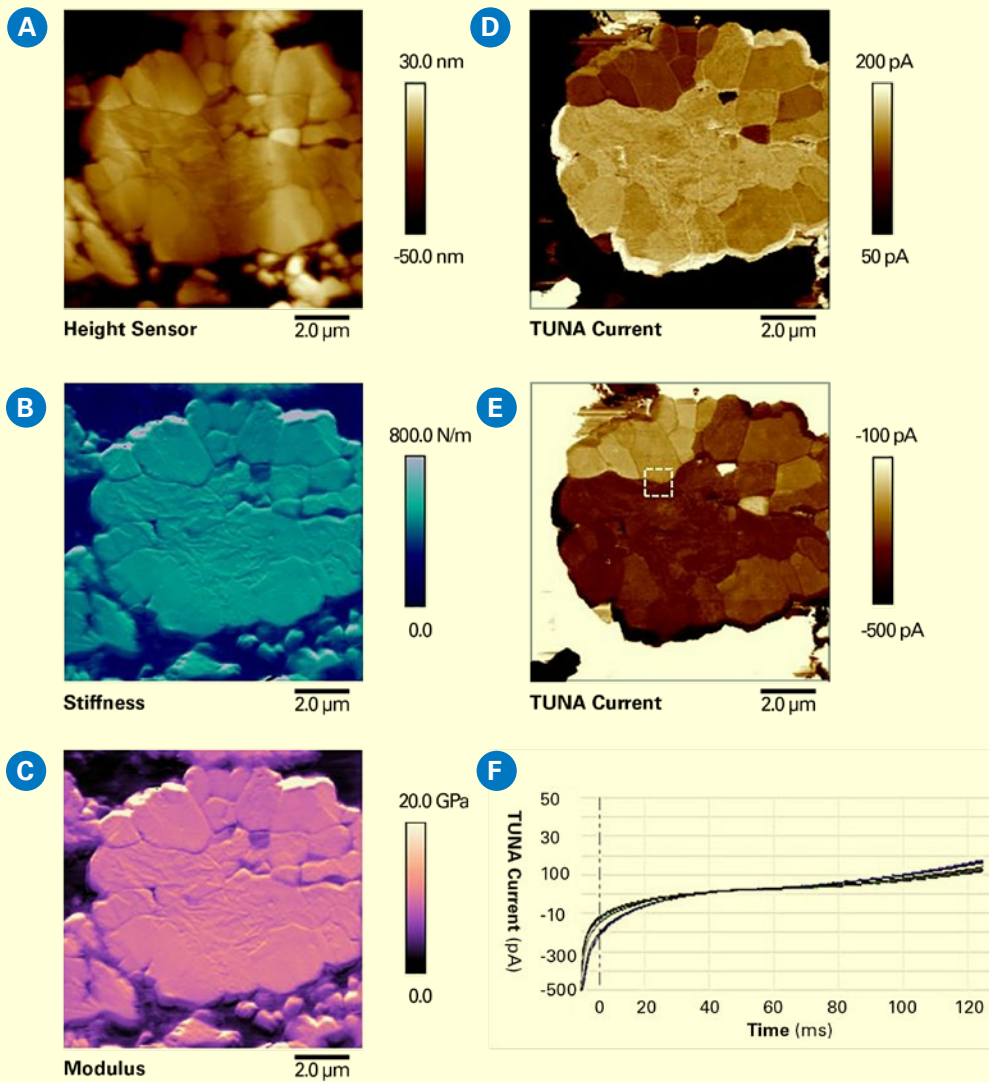


Figure 13. DCUBE-TUNA studies of a Li metal oxide grain on a battery cathode consisting of Li metal oxide, polymer binder, and conductive carbon nanoparticles: (a) surface topography; (b) map of quantitative surface stiffness differentiating different domains; (c) quantitative modulus map; (d)-(e) two slices from spectroscopic mapping showing TUNA current image at a sample bias of +4 V and -4 V, respectively; and (f) all current-time spectra from the area indicated by the white square in (e). During this 125 ms dwell period, the sample bias sweeps linearly from -4 V to +4 V, or at a rate of  $64\ \text{V}\cdot\text{s}^{-1}$ .

## Case Study 2:

### DataCube Scanning Capacitance Microscopy of Semiconductor Devices

Scanning capacitance microscopy (SCM) provides a method for direct measurement of activated carrier concentration with nanometer-scale accuracy in two dimensions. In SCM, the variation in carrier concentration inside semiconductor structures can be imaged through measurement of the  $dC/dV$  signal of the metal-oxide-semiconductor (MOS) capacitor formed by the probe and the semiconductor sample. In this mode, the probe is scanned in contact mode, and topography and electrical data are acquired simultaneously, enabling the direct correlation of a sample location with its electrical properties. Applications of SCM include failure analysis of semiconductor devices and two-dimensional carrier profiling of cross-sectioned semiconductor devices.

Conventional SCM has two limitations: first, as it operates in contact mode, it can suffer from high imaging and shear forces, which links directly to tip lifetime, especially on structures with substantial topography variations. Second, it is operating at a fixed DC bias voltage between the tip and the sample, while lots of information becomes visible only when operating at a variety of voltages. In fact, cycling DC bias on every pixel has been a topic of interest for quite some time. DCUBE-SCM overcomes these two limitations by providing high spatial and spectral resolution spectroscopic mapping data without the use of contact mode. By further analysis of the resulting data cubes, researchers can obtain additional information on oxide thickness, oxide charges, threshold voltages, contamination from mobile ions, and interface trap densities.

Figure 14 shows a DCUBE-SCM example from a SRAM transistor. In this measurement, the DC sample voltage was swept from  $-2\text{ V}$  to  $2\text{ V}$ . The scan size was  $2 \times 2\ \mu\text{m}^2$  with  $128 \times 128$  pixels. Each pixel took  $100\text{ ms}$  and the whole data cube was collected in  $27\text{ min}$ . Both the SCM  $dC/dV$  amplitude (displayed in Figure 14) and  $dC/dV$  phase data were also stored, in addition to the force-distance data. Visualization of the  $dC/dV$  amplitude data cube in a three-dimensional (3D) space of  $X$ ,  $Y$  and  $V_{DC}$  was created in MATLAB, shown in Figure 14a. The vertical plane shown in Figure 14b is a slice displaying the dynamic change of  $dC/dV$  amplitude with  $V_{DC}$  along the line in the  $X$  direction. This slice shows how the pnp junction carrier profile varies with

the DC sample voltage and is a demonstration of the movement of apparent junction, that is, effective channel length with DC voltage. Slices extracted at fixed DC voltages are shown in Figures 14c to 14k, where the fixed DC voltage is indicated on each image. Figures 14e and 14i shows a defect on the right pnp junction. Interestingly, this defect is only visible at certain voltages, as shown in this series of data. This defect is better displayed by a movie of the whole collection of 128 slices.

This example illustrates that DataCube imaging allows one to observe effects easily missed when using conventional electrical modes operated at only a few discrete operating conditions.

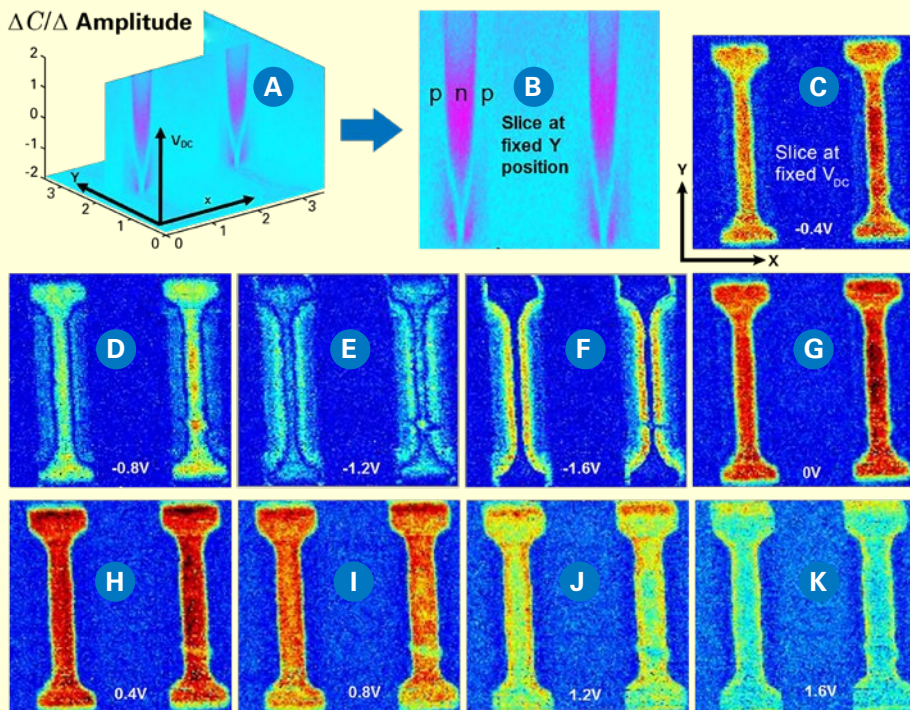


Figure 14. DCUBE-SCM study of two adjacent SRAM pnp transistors. This collection of images displays the SCM  $dC/dV$  amplitude data: (a) data cube in a 3D space of X, Y and  $V_{DC}$ ; (b) a slice of the data cube at a fixed Y position; (c)-(k) slices at selected, fixed DC biases along the  $V_{DC}$  coordinate. DC sample voltage was swept from -2 V to +2 V. The scan size is  $2 \times 2 \mu\text{m}^2$  with  $128 \times 128$  pixels.

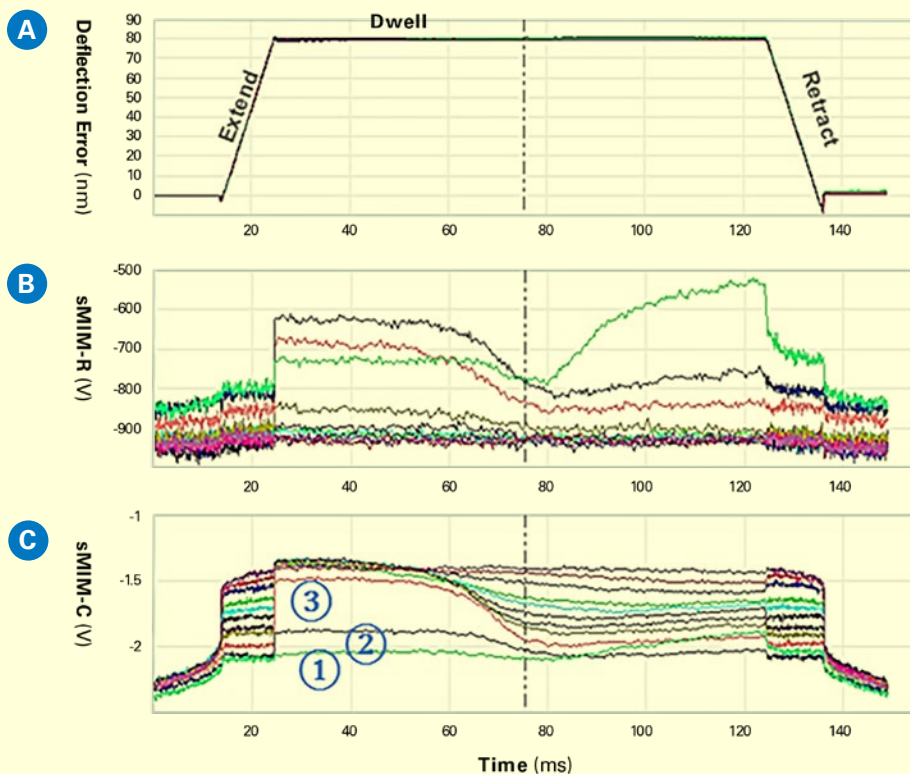
## Case Study 3:

### DataCube Scanning Microwave Impedance Microscopy on Delicate Samples

In scanning microwave impedance microscopy (sMIM), a microwave signal reflected from the tip-sample interface holds information of the electrodynamic properties of the sample surface underneath the tip apex. Detecting and processing the reflectance in real time allows sMIM to directly access the permittivity and conductivity of the material. When an AFM-type sMIM probe is scanning across the sample surface, sMIM is capable of imaging variations in resistive (sMIM-R) and capacitive (sMIM-C) properties. This detection approach does not require making electrical contact between the sample and the substrate, as sMIM is based on the capacitive coupling between the tip and the sample. By AC-biasing the sample, sMIM also provides carrier profiling (dC/dV) capability similar to traditional SCM. In the same way, it also uniquely offers mapping of nonlinear resistive properties (dR/dV). With both DC and AC sMIM signals, sMIM is suitable for studying surfaces with complex composition and over a broad dynamic range, e.g., metallic, semiconducting and insulating domains. As a near field method, the resolution of sMIM is limited by the tip radius of the probe and it can easily achieve a lateral resolution of <30 nm for electrical mapping. Sub-aF sensitivity and high signal/noise ratios are realized by using waveguide tips with coaxial shielding. When combined with PeakForce Tapping, it is possible to obtain sMIM results on delicate samples, such as carbon nanotubes, and simultaneously acquire mechanical sample properties, such as modulus and adhesion. With DCUBE-sMIM one can acquire the same properties at a variety of sample voltages, in a single scan and get the full picture at once.

Figure 15 shows typical data extracted from a DCUBE-sMIM study. In this example, Si sample with a n-type and p-type staircase carrier profile was used, which forms a candidate sample for quantification of AFM-based carrier profiling methods.<sup>30</sup> Both the C-V spectra (sMIM-C vs sample bias) and R-V spectra (sMIM-R vs sample bias) were collected within 100 ms per pixel, covering a bias range of -2 V to +2 V. Having images over this bias range helps to differentiate and locate all carrier levels and regions in the sample. This is seen in the sMIM-C data in Figure 15. The negative bias in Figure 15a drives the p-type regions into depletion regime, enhancing their contrast.

Figure 15. DCUBE-sMIM study of a Si sample with n-type and p-type staircase carrier profile: (a)–(c) ‘sMIM-C’ capacitance image slices at selected sample biases.



The n-type regions are in the inversion regime, depressing their contrast, while the positive bias in Figure 15c has the opposite effect.

DCUBE-sMIM provides valuable nanoelectrical information not only during the surface hold time, but also during the approach and retract processes. This is seen in Figure 16, which are spectra taken at the locations marked by X in Figure 15b. First, during the hold time, the sMIM-C signals in Figure 16b show a gradual change in slope with carrier density. Most curves were taken in the p-type region. At negative bias, the sample is in the accumulation regime, causing equally high sMIM-C signal, which then drops as the bias turns positive and the sample goes into depletion. The signal drops further

for lower doped regions. Second, Figure 16b and 16c also capture the sMIM signals before the probe touches and before bias is applied, thus automatically capturing the distance dependence.

Figure 17 combines the information in Figures 15 and 16 into a single spatio-spectral slice. Fitting of the sMIM-C versus distance spectra allows extraction of tip-shape information. One can easily extract the capacitance image at a given, fixed height above the sample. This image represents the background or stray capacitance and can be subtracted from all capacitance data

to remove background effects. This enhances the sMIM-C data, removes any stray capacitance effects, and provides a path for quantification of the sMIM-C data. Detailed analysis and comparison of the sMIM signal during the extend and retract period also provides additional information. For example, asymmetric behaviors indicate a change of the sample surface after the dwell time.

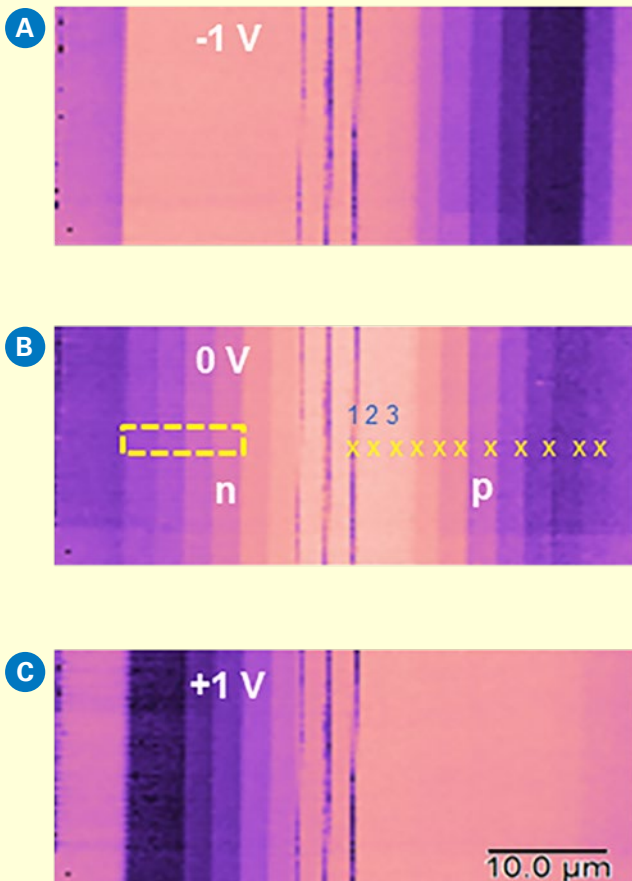


Figure 16. Eleven spectral sets of force, sMIM-R and sMIM-C, respectively, collected at user-selected positions marked on Figure 15b.



As seen in this case study, DataCube technology has allowed for the simultaneous collection of data. It also provides it in an easy-to-use manner that can make differences in surfaces more evident after all of the data collected is combined.

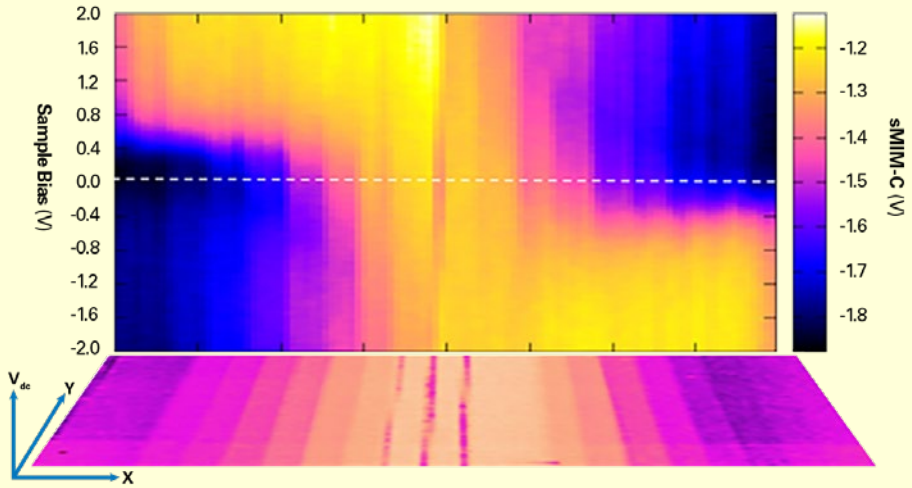


Figure 17. Slice image representing the sMIM-C signal vs sample bias and X position at a fixed Y location.

# Case Study 4:

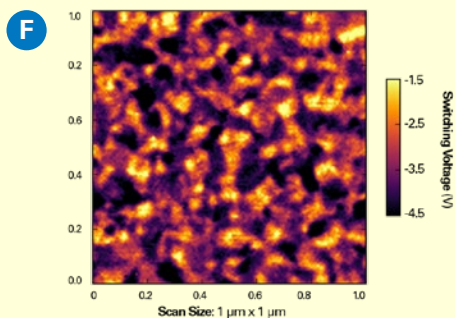
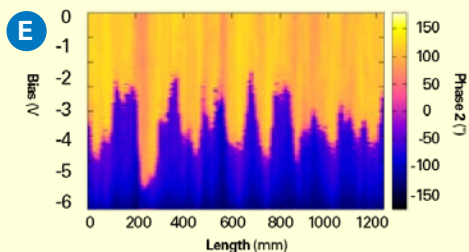
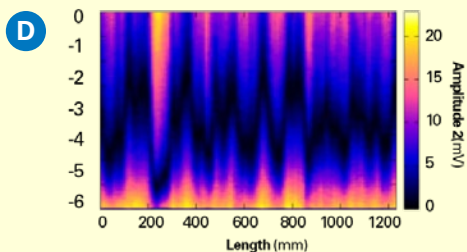
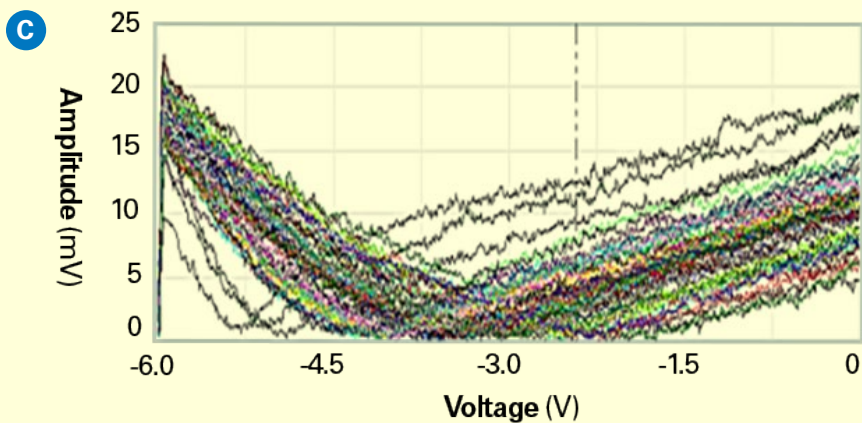
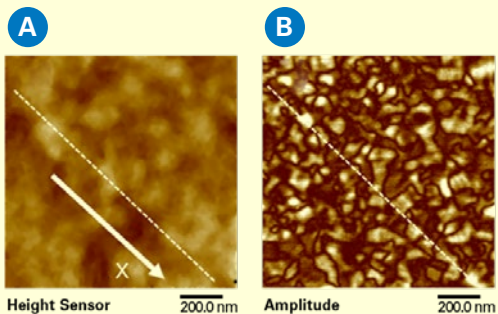
## DataCube Piezoresponse Microscopy on Piezoelectric Films

DataCube Piezoresponse Microscopy (DCUBE-PFM) has, once again, the benefit of not damaging the surface that it is imaging like normal contact mode approaches. Beyond this, DCUBE-PFM allows for in-depth three-dimensional imaging of piezoelectric films. This case study explores some different uses of DataCube technology with piezoresponsive material.

Piezoresponsive materials are substances that undergo mechanical deformation in response to an applied voltage. The properties of piezoresponsive materials make them useful in a wide range of areas, from microelectromechanical systems (MEMS) to biosensors. Ferroelectric materials are a subset of piezoelectrics that have particularly advantageous functional properties. As process control improves and fabrication of small-volume ferroelectrics becomes more common, researchers have discovered that the physical characteristics of these materials change as they shrink. PFM enables high-resolution nanoscale characterization of piezoresponsive materials and topographical imaging. PFM is a contact AFM technique to measure sample displacement in response to an applied AC bias. The resulting cantilever deflection of the probe in contact with the sample is detected then demodulated by use of a lock-in amplifier, such that topography and ferroelectric domains can be imaged simultaneously with high resolution. PFM has also been widely used for domain writing and ferroelectric switching studies.<sup>31-33</sup> Integration with the DataCube technique, DCUBE-PFM, enables simultaneous acquisition of nanomechanical mapping and PFM amplitude/phase spectra in every pixel, revealing the switching behavior of each individual domain in a single data set. In addition, DCUBE-PFM overcomes artifacts, sample damage, and complexity of data analysis associated with the conventional contact mode-based approach.

Figure 18 shows an example of DCUBE-PFM studies of a BiFeO<sub>3</sub> (BFO) piezoelectric film. In this experiment, the sample voltage is ramped from -6 V to 0 V during the dwell period while collecting the PFM amplitude and phase signals. Figure 18a shows the surface topography; a flat film with roughness of 0.37 nm. A PFM amplitude slice at -4.5 V differentiates different piezoelectric domains (Figure 18b). Figure 18c shows the first 50 of the selected 110 spectra along a 1.2 μm long line, as indicated by the

Figure 18. DCUBE-PFM studies of a BiFeO<sub>3</sub> (BFO) piezoelectric film: (a) height; (b) PFM amplitude image; and (c) 50 of the selected 110 spectra along a 1.2  $\mu\text{m}$  long line as indicated in (a) and (b), crossing multiple domains in a BFO ferro-electric sample; (d) and (e) plots of those 110 spectra show both PFM amplitude and PFM phase vs. bias during a ramp from -6 V to 0 V; (f) map of switching voltages extracted from the data cube.



white dashed lines in Figures 18a and 18b, crossing multiple domains in this BFO ferroelectric sample. These spectra indicate distinct switching voltages among different domains as the minimum of each spectrum spreads from about -5.0 V to -2.0 V on Figure 18c. These switching voltages can be extracted for each individual domain by the analysis of the spectra. Figures 18d and 18e are color plots of those 110 amplitude and phase spectra, respectively. The abrupt changes in color along the voltage (vertical) direction show the locations of the switching voltages. Further analysis of the data cube enables the extraction of the switching voltage at every pixel. These switching voltages can be plotted in a new map (Figure 18f) that shows that heterogeneous piezoelectric properties are present between domains and also within some single domains.

Figure 19 presents the same data cube results in a different format. Figures 19a and 19b respectively show two sets of amplitude and phase spectra from two domains. Sample biases for the minimum of the amplitude spectra or the rise of the phase spectra indicate the switching voltages for the corresponding pixel on the XY plane. Figure 19c and 19d show the amplitude and phase data cubes, respectively. The horizontal directions, X and Y, correspond to the scan area of the sample, which is  $1 \times 1 \mu\text{m}^2$ . The vertical direction, Z, from bottom to the top, is following the time of the hold segment while the sample bias was linearly applied from -6 V to 0 V. The size of this cube is  $128 \times 128 \times 833$  pixels. The four horizontal planes correspond to the slices of amplitude or phase at different sample biases. To better show the domain boundaries, the middle slice in the phase cube is shown as a set of contours over the range of values appearing at this bias. The two vertical slices along the XZ direction represent amplitude or phase changing over the sample bias (Z direction) along two line positions in the XY plane. Figures 19e through 19i are slices of amplitude at different sample bias, extracted from data cube.

This case study exemplifies the detail with which DataCube technology is able to collect three-dimensional data and create three-dimensional visuals. The biggest reason for this is the ability to change voltage at every pixel, a function unique to DataCube technology.

Figure 19. DCUBE-PFM studies of a BiFeO<sub>3</sub> (BFO) piezoelectric film: (a) two sets of amplitude spectra from two different domains inside the yellow circles in (f) and (h); (b) corresponding phase spectra to those in (a); (c) and (d) are cubes of the amplitude and phase data, respectively. X and Y correspond to the 1x1  $\mu\text{m}$  scan area. The vertical direction, Z, from bottom to the top, is the sample bias from -6 V to 0 V. The cube color represents the amplitude or phase in the cube space, i.e., the measured PFM signal at a specific XY location and applied bias. The cube size is 128x128x833 (or 1x1  $\mu\text{m}^2 \times 6 \text{ V}$ ). The four horizontal planes correspond to the slices of amplitude or phase at different sample bias. The middle slice in the phase cube is shown as a set of contours over the range of values appearing at this bias. The two vertical slices along the XZ direction represent amplitude or phase changing over the sample bias (Z direction) along two line positions in the XY plane.

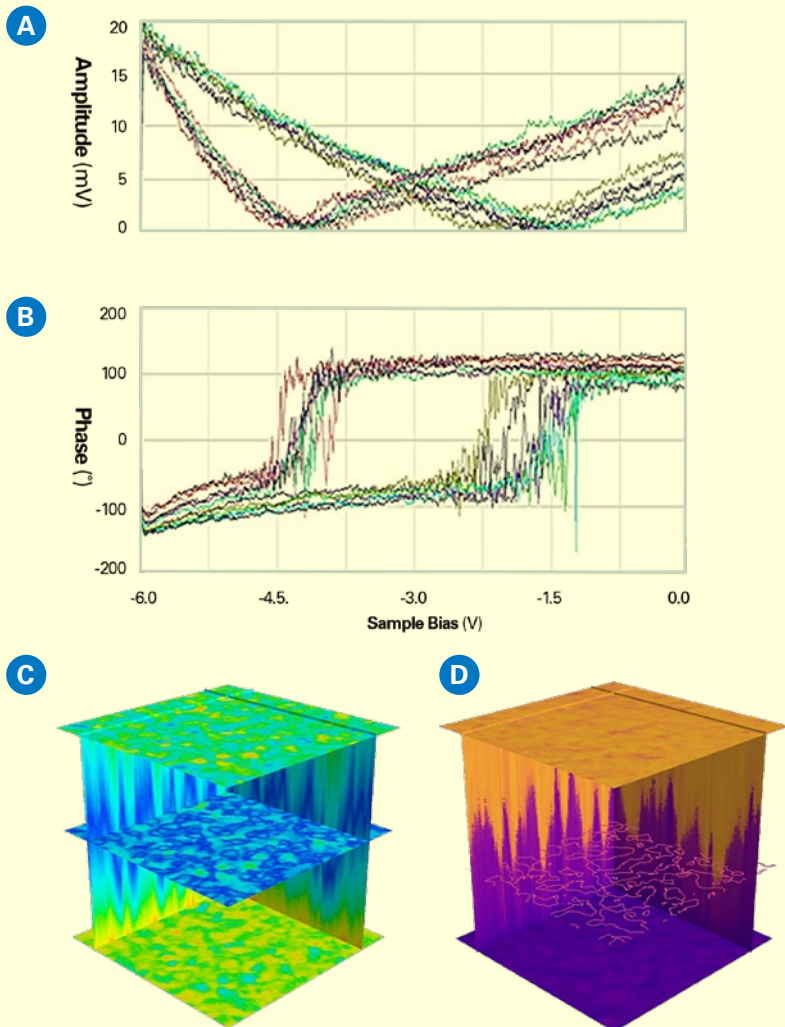
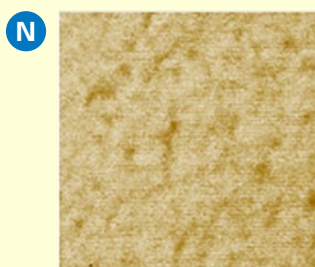
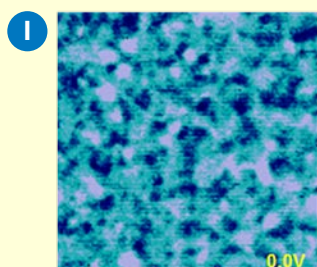
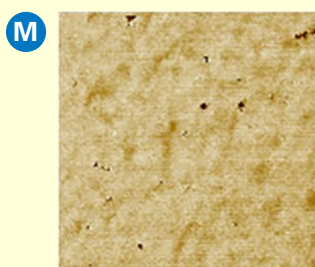
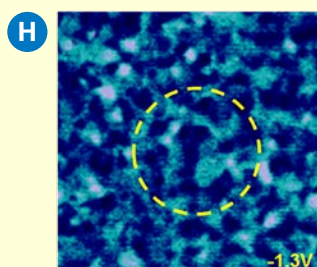
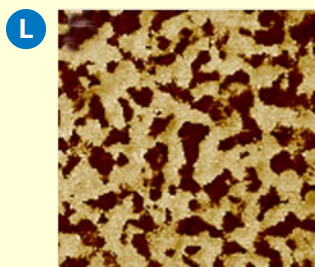
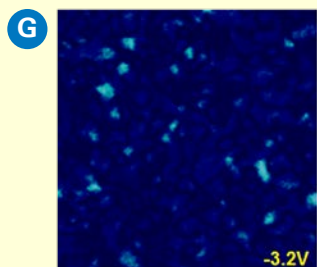
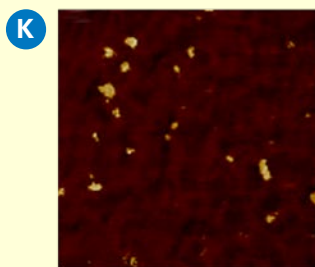
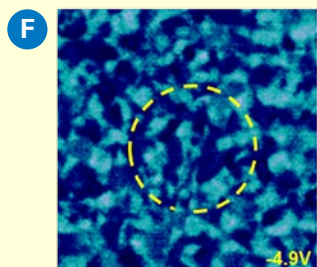
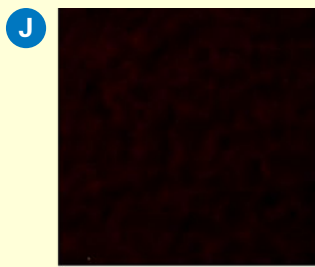
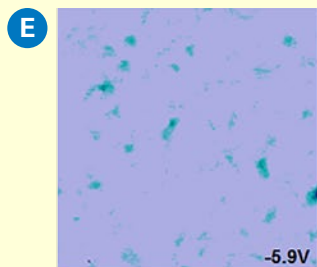


Figure 19 continued.  
(e)-(i) are slices of amplitude at different sample bias; and (j)-(n) are slices of phase at different sample bias.





## Case Study 5:

### DataCube – Contact Resonance PFM on a LiTaO<sub>3</sub> Sample

This case study discusses the way that Bruker has combined DataCube technology and PFM with FASTForce Volume Contact Resonance mode (FFV-CR).

In PFM, the applied AC bias of a certain frequency results in a periodic AC deformation of the sample surface at the same frequency. Operation at or near the contact resonance has been exploited in PFM to provide enhanced piezoelectric response signal. For a single-frequency PFM measurement, the implementation of this technique is limited, as the contact resonance shifts with the nature of the tip-sample contact as well as with the sample material properties. DCUBE-CR PFM overcomes this challenge, where during the dwell duration the frequency is swept to collect a complete contact resonance spectrum. This hybrid mode inherits all advantages from the FFV-CR developed for characterization of viscoelastic mechanical properties:

- frequency sweeps can be performed over a broad range (up to 5 MHz) enabling observation and tracking of multiple eigenmodes at once;
- resonance frequency and quality factor can be extracted with a real-time fit of the spectrum, and can be calculated into loss modulus, storage modulus, and loss tangent when applying the proper mechanical model;
- adhesion, stiffness and modulus are extracted out of the force-distance spectrum; and
- piezoelectric properties can be extracted out of the phase and amplitude signals, in particular at the resonance frequency.

Figures 20a to 20c show some typical DCUBE-CR PFM force ramping, PFM phase, and PFM amplitude spectra of a LiTaO<sub>3</sub> (LTO) sample. In this measurement, the frequency was ramped from 250 to 400 kHz in every pixel during a 100 ms dwell period. Figures 20d and 20e show the phase and amplitude data cubes, respectively. The size and the space pixel density of these two cubes are 3x3 μm<sup>2</sup> x 150 kHz and 256x256x260. The horizontal planes show phase (Figure 20d) or amplitude (Figure 20e) maps at specific frequencies, where different piezoelectric domains are well differentiated



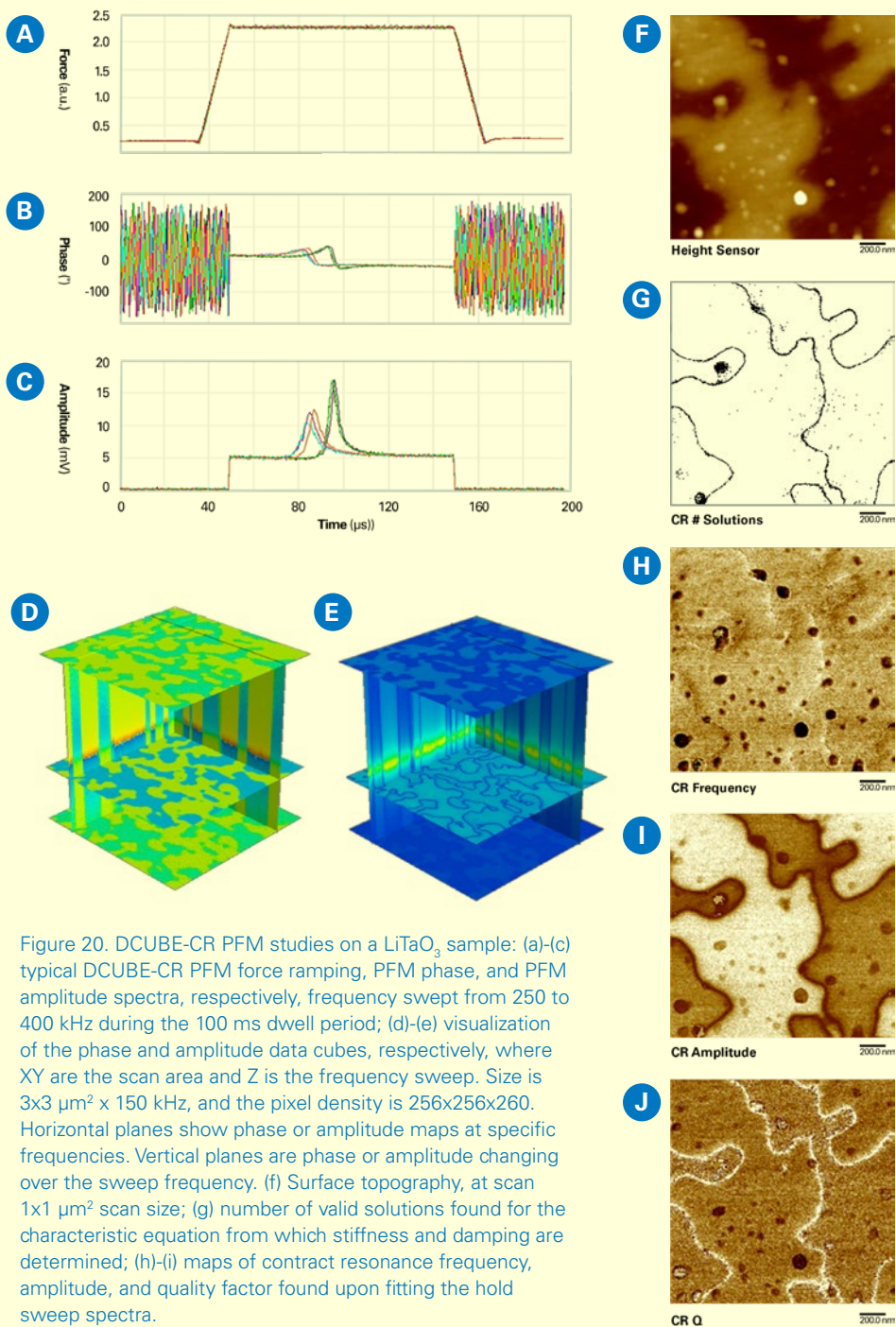


Figure 20. DCUBE-CR PFM studies on a  $\text{LiTaO}_3$  sample: (a)-(c) typical DCUBE-CR PFM force ramping, PFM phase, and PFM amplitude spectra, respectively, frequency swept from 250 to 400 kHz during the 100 ms dwell period; (d)-(e) visualization of the phase and amplitude data cubes, respectively, where XY are the scan area and Z is the frequency sweep. Size is  $3 \times 3 \mu\text{m}^2 \times 150 \text{ kHz}$ , and the pixel density is  $256 \times 256 \times 260$ . Horizontal planes show phase or amplitude maps at specific frequencies. Vertical planes are phase or amplitude changing over the sweep frequency. (f) Surface topography, at scan  $1 \times 1 \mu\text{m}^2$  scan size; (g) number of valid solutions found for the characteristic equation from which stiffness and damping are determined; (h)-(i) maps of contract resonance frequency, amplitude, and quality factor found upon fitting the hold sweep spectra.

at and near contact resonance. Vertical planes are phase (Figure 20d) or amplitude (Figure 20e) changing with the sweep frequency, which demonstrates shifts in the contact resonance frequency between different domains. Figures 20f through 20j show the DCUBE-CR PFM data on the same LiTaO<sub>3</sub> sample with a smaller scan size of 1x1 μm<sup>2</sup>. Figure 20f is the surface topography with a roughness (Rq) of ~1.5 nm. Figure 20g shows the number of peaks that the algorithm found during the fitting. At the domain boundaries and in some contaminant positions, this signal becomes zero indicating that the material does not show piezoelectric response. The *CR Frequency*, *CR Amplitude*, and *CR Q channels* in (h)-(i) are maps of contact resonance frequency, amplitude, and quality factor found upon fitting the hold sweep spectra. This example demonstrates that DCUBE-PFM, in conjunction with contact resonance, provides the full benefits of DCUBE-PFM with the added benefits of providing a frequency ramp at every pixel, which in turn provides a full spectrum and the peak sensitivity at the contact resonance.

This final case study demonstrates that DCUBE-PFM combined with contact resonance can provide an incredibly full spectrum of three-dimensional data. Just as with the previous case studies, the use of DataCube technology has enhanced a previously strong nanoelectrical mode to make it even stronger.



## Citations

1. Pittenger, B., Erina, N., and Su, C., "Quantitative Mechanical Property Mapping at the Nanoscale with PeakForce QNM," Bruker Application Note 128 (2012).
2. Pittenger, B. and Yablon, D. G., "Improving the Accuracy of Nanomechanical Measurements with Force-Curve-Based AFM Techniques," Bruker Application Note 149 (2017).
3. Berquand, A., "Quantitative Imaging of Living Biological Samples by PeakForce QNM Atomic Force Microscopy," Bruker Application Note 135 (2011).
4. Kaemmer, S. B., "Introduction to Bruker's ScanAsyst and PeakForce Tapping AFM Technology," Bruker Application Note 133 (2011).
5. Pittenger, B. and Yablon, D. G., "Quantitative Measurements of Elastic and Viscoelastic Properties with FASTForce Volume CR," Bruker Application Note 148 (2017).
6. Li, C., Minne, S., Pittenger, B., and Mednick, A., "Simultaneous Electrical and Mechanical Property Mapping at the Nanoscale with PeakForce TUNA." Bruker Application Note 132 (2011).
7. Li, C. et al., "PeakForce Kelvin Probe Force Microscopy," Bruker Application Note 140 (2013).
8. Huang, Z. et al., "Nanoscale Mapping of Permittivity and Conductivity with Scanning Microwave Impedance Microscopy," Bruker Application Note 145 (2016).
9. Calahorra, Y., Smith, M., Datta, A., Benisty, H., and Kar-Narayan, S., "Mapping Piezoelectric Response in Nanomaterials Using a Dedicated Non-Destructive Scanning Probe Technique," *Nanoscale* 9, 19290-97 (2017).
10. Huang, Z. et al., "An Introduction to AFM-Based Scanning Electrochemical Microscopy: PeakForce SECM," Bruker Application Note 147 (2017).
11. Jiang, J. J. et al., "Nanoelectrical and Nanoelectrochemical Imaging of Pt/p-Si and Pt/p+-Si Electrodes," *ChemSuschem* 10, 4657-63 (2017).
12. Nellist, M. R. et al., "Atomic Force Microscopy with Nanoelectrode Tips for High Resolution Electrochemical, Nanoadhesion and Nanoelectrical Imaging," *Nanotechnology* 28, 095711 (2017).
13. Nellist, M. R. et al., "Potential-Sensing Electrochemical Atomic Force Microscopy for in operando Analysis of Water-Splitting Catalysts and Interfaces. *Nat Energy* 3, 46-52 (2018).
14. Toma, F. M., "Disentangling Interfacial Energetics," *Nat Energy* 3, 6-7 (2018).

15. Edwards, H. et al., "Scanning Capacitance Spectroscopy: An Analytical Technique for pn-Junction Delineation in Si Devices," *Appl Phys Lett* 72, 698-700 (1998).
16. Yang, S. M. et al., "Humidity Effect on Nanoscale Electrochemistry in Solid Silver Ion Conductors and the Dual Nature of Its Locality," *Nano Lett* 15, 1062-69 (2015).
17. De Wolf, P. et al., "Data Cube Modes: Enabling Functional Imaging with Higher Dimensional Electrical Data Sets," *Microscopy Today* (2018).
18. Palacin, M. R. and de Guibert, A., "Why Do Batteries Fail?" *Science* 351, 1253292 (2016).
19. Semenov, A. E., Borodina, I. N., and Garofalini, S. H., "In Situ Deposition and Ultrahigh Vacuum STM/AFM Study of V2O5/Li3PO4 Interface in a Rechargeable Lithium-Ion Battery," *J Electrochem Soc* 148, A1239-46 (2001).
20. Becker, C. R., Prokes, S. M., and Love, C. T., "Enhanced Lithiation Cycle Stability of ALD-Coated Confined a-Si Microstructures Determined Using In Situ AFM," *ACS Appl Mater Inter* 8, 530-37 (2016).
21. Hernandez, G. et al., "Redox-Active Polyimide-Polyether Block Copolymers as Electrode Materials for Lithium Batteries," *Rsc Adv* 5, 17096-103 (2015).
22. Hiesgen, R. et al., "AFM As an Analysis Tool for High-Capacity Sulfur Cathodes for Li-S Batteries," *Beilstein J Nanotech* 4, 611-24 (2013).
23. Chen, J. C., Yan, Y. D., Sun, T., Qi, Y., and Li, X. D., "Deformation and Fracture Behaviors of Microporous Polymer Separators for Lithium Ion Batteries," *Rsc Adv* 4, 14904-14 (2014).
24. Breitung, B., Baumann, P., Sommer, H., Janek, J., and Brezesinski, T., "In Situ and Operando Atomic Force Microscopy of High-Capacity Nano-Silicon Based Electrodes for Lithium-Ion Batteries," *Nanoscale* 8, 14048- 56 (2016).
25. Shen, C. et al., "Direct Observation of the Growth of Lithium Dendrites on Graphite Anodes by Operando EC-AFM," *Small Methods* 2, 1700289 (2018).
26. Wang, S. W. et al., "Operando Study of Fe3O4 Anodes by Electrochemical Atomic Force Microscopy," *Appl Surf Sci* 426, 217-23 (2017).
27. Kumar, R. et al., "In Situ and Operando Investigations of Failure Mechanisms of the Solid Electrolyte Interphase on Silicon Electrodes," *ACS Energy Lett* 1, 689-97 (2016).
28. Wang, S. W., Yang, K., Gao, F., Wang, D. Y., and Shen, C., "Direct Visualization of Solid Electrolyte Interphase on Li4Ti5O12 by In Situ AFM," *Rsc Adv* 6, 77105-10 (2016).

29. Kitta, M. and Kohyama, M., "Stability of the LiMn<sub>2</sub>O<sub>4</sub> Surface in a LiPF<sub>6</sub>-Based Non-Aqueous Electrolyte Studied by In-Situ Atomic Force Microscopy," *Jpn J Appl Phys* 55 (2016).
30. Schweinbock, T. and Hommel, S., "Quantitative Scanning Microwave Microscopy: A Calibration Flow," *Microelectron Reliab* 54, 2070-74 (2014).
31. Gruverman, A., Auciello, O., and Tokumoto, H., "Imaging and Control of Domain Structures in Ferroelectric Thin Films Via Scanning Force Microscopy," *Ann Rev Mater Sci* 28, 101-23 (1998).
32. Wang, C. S. et al., "Ferroelastic Switching in a Layered-Perovskite Thin Film," *Nat Commun* 7, 10636 (2016).
33. C., A. J. et al., "Machine Detection of Enhanced Electromechanical Energy Conversion in PbZr<sub>0.2</sub>Ti<sub>0.8</sub>O<sub>3</sub> Thin Films," *Advanced Materials* 30, 1800701 (2018).



